Diamond & Related Materials xxx (2008) xxx–xxx

Contents lists available at ScienceDirect

Diamond & Related Materials

journal homepage: www.elsevier.com/locate/diamond

Structural and magnetic resonance study of astralen nanoparticles

A.I. Shames [a,*], E.A. Katz [b,c], A.M. Panich [a], D. Mogilyansky [d], E. Mogilko [e], J. Grinblat [f], V.P. Belousov [g], I.M. Belousova [g], A.N. Ponomarev [h]

[a] Department of Physics, Ben-Gurion University of the Negev, Be'er-Sheva 84105, Israel
[b] Department of Solar Energy and Environmental Physics, J. Blaustein Institutes for Desert Research, Ben-Gurion University of the Negev, Sede Boqer 84990, Israel
[c] Ilse-Katz Center for Meso- and Nanoscale Science and Technology, Ben-Gurion University of the Negev, Be'er-Sheva 84105, Israel
[d] Institutes for Applied Research, Ben-Gurion University of the Negev, Be'er-Sheva 84105, Israel
[e] Department of Physics and Center for Superconductivity, Bar-Ilan University, Ramat Gan 52900, Israel
[f] Department of Chemistry, Bar-Ilan University, Ramat Gan 52900, Israel
[g] Institute for Laser Physics, SIC Vavilov SOI, St. Petersburg 199034, Russia
[h] JSC Astrin-Holding, St. Petersburg 198095, Russia

ARTICLE INFO

Available online xxxx

Keywords:
Carbon nanoparticles
Multi-shell polyhedra
Magnetic resonance

ABSTRACT

Using HRTEM, XRD and Raman spectroscopy we demonstrated a polyhedral multi-shell fullerene-like structure of astralen particles. The polyhedra consist of large defect-free flat graphitic faces connected by defective edge regions with presumably pentagon-like structure. The faces comprise a stacking of 20–50 planar graphene sheets with inter-sheet distance of ~0.340 nm. Average sizes of the particles and their flat faces are of ~40 nm and ~15 nm, respectively. EPR spectra of astralen powder reveal two components: a very broad signal with $\Delta H_{pp}<1$ T and an asymmetric narrow one centered close to $g=2.0$. The latter consists of two overlapping Lorentzian lines. All spectral components are independent of the ambient pressure. The intensities of all EPR signals show no changes on decreasing temperature from $T=300$ K down to 4 K demonstrating the Pauli paramagnetism. Temperature dependent ^{13}C NMR measurements yield nuclear spin-lattice relaxation times $T_{1n}\sim T^{-0.612}$. The exponent in the temperature $T_{1n}(T)$-dependence for astralen falls between the metallic behavior, $T_{1n}\sim T^{-1}$ (Korringa relation), and the semiconductor behavior, $T_{1n}\sim T^{-0.5}$. The unusual magnetic resonance features are attributed to delocalized charge carriers which amount considerably exceeds that of spins localized in defects on astralen edges.

1. Introduction

Carbon is a unique element existing in a wide variety of stable forms ranging from insulator/semiconducting diamond to metallic/semimetallic graphite. The discovery [1] of *buckminsterfullerene*, C_{60}, a new variety of carbon, has generated enormous interest in many areas of physics, chemistry and material science. Furthermore, it turns out that C_{60} is only the most abundant member of an entire class of fully conjugated, all-carbon molecules—the fullerenes (C_{20},C_{24},C_{26}…C_{60}…C_{70},C_{72},C_{74}…carbon nanotubes). It is already clear from the vast and increasing literature on fullerene-based materials that much complex and fascinating physics lies behind the geometrical simplicity of these structures. Now, term *fullerenes* is used for various all-carbon closed-cage molecules in which π-conjugated carbon hexagon rings are condensed to form a closed surface with the participation of pentagon rings. By the other words, fullerenes can be considered as small pieces of graphite acquired curvature due to the presence of pentagonal rings in the hexagonal graphitic sheet. Topological analysis on the base of the Euler's theorem for convex polyhedra [2] shows that any fullerene molecule must have 12 pentagonal faces and the number of hexagonal faces is arbitrary.

Recently, much attention has turned towards novel fullerene-related materials, carbon *nanocapsules* or carbon *onions* that consist of concentric fullerene-like shells. The formation of carbon onions was first reported by Ugarte [3]. He observed that carbon soot particles and tubular graphitic structure are transformed into quasi-spherical carbon onions by intense electron-beam irradiation in a transmission electron microscope. Structure of spherical onions cannot be described in terms of perfect fullerene-like shells made of pentagonal and hexagonal carbon rings only and requires introduction of large number of defects, heptagonal–pentagonal pairs, for example [4]. As a result, π-electrons in spherical onions are localized in very small domains of sp^2 graphitic sheets, and do not act as conduction electrons [5]. On the contrary, polyhedral onions have ordered graphitic structure presumably with defect-free sp^2 flat faces and definite number of pentagon-like defects condenses at the polyhedral cusps [6]. Accordingly, delocalized π-electrons in polyhedral onions can act as conduction electrons. This effect should be enhanced as

* Corresponding author.
E-mail address: sham@bgu.ac.il (A.I. Shames).

0925-9635/$ – see front matter © 2008 Published by Elsevier B.V.
doi:10.1016/j.diamond.2008.10.056

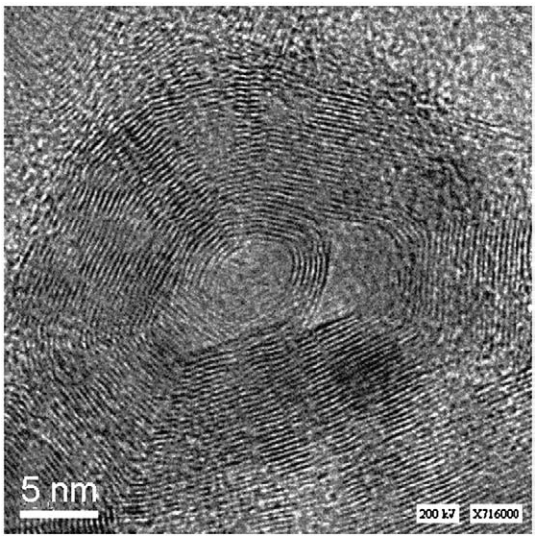

Fig. 1. Representative HRTEM image of astralen particles.

sizes of polyhedra increase. Unfortunately, knowledge on the correlation between structure and electronic properties of individual carbon onions is very limited. To the best of our knowledge, such comprehensive studies were performed only for spherical and small polyhedral onions produced by high temperature (HT) vacuum annealing of nanodiamond particles [5,7–9].

For the present study we adopted large carbon particles, so-called astralens, produced by arc discharge of graphite [10]. Although delocalization of π-electrons might be considered as a prerequisite for the recently reported applications of astralen in nonlinear optics [11–13], their polyhedral fullerene-like structure has not been confirmed so far. We provided such a confirmation using High Resolution Transmission Electron Microscopy (HRTEM), X-ray Diffraction (XRD) and Raman spectroscopy studies. By means of Electron Paramagnetic Resonance (EPR) and Nuclear Magnetic Resonance (NMR) spectroscopies we investigated electronic properties of astralen in comparison with the reported data for their spherical and small polyhedral cousins obtained from HT treated (HTT) nanodiamonds [5,8,9]. Our results verify a hypothesis that each astralen nanoparticle constitutes a closed network of delocalized π-electrons.

2. Experimental details

Astralen particles were produced by thermal vaporization of graphite anode by arc discharge using special conditions of vaporization, extraction and subsequent treatment of cathodic deposit [10].

Graphite powder produced from pulverized Alpha Aesar graphite rod (99%) was used as reference sample in all of our investigations.

Structure of astralen particles was studied by HRTEM, XRD and Raman spectroscopy. The HRTEM images were taken with JEOL 2011 microscope having an acceleration voltage of 200 kV. The XRD data were collected on Philips 1050/70 powder diffractometer using CuK_{α}-radiation and operating at 40 kV/30 mA. The XRD diffraction patterns were then treated using the FULLPROF program in order to derive positions and widths of X-ray reflections.

Raman spectra were recorded with a Jobin-Yvon LabRam HR 800 micro-Raman system, equipped with a liquid-N_2-cooled detector. The excitation wavelength was He–Ne laser supplied with the JY Raman spectrometer (633 nm). The measurements were taken with the 600 g mm^{-1} grating and a microscope confocal hole setting of 100 μm, giving a resolution of 4–8 cm^{-1}. Laser intensity on the sample was 3 mW; the spot size is about 20 μm^2.

EPR measurements within the temperature range 4 K≤T≤300 K were carried out using a Bruker EMX-220 X-band (ν~9.4 GHz) spectrometer equipped with an Oxford Instrument ESR900 cryostat and an Agilent53150A frequency counter. Temperature dependences of the following EPR spectra parameters were analyzed: resonance field H_r, peak-to-peak line width ΔH_{pp} and doubly integrated intensity (DIN), proportional to the EPR susceptibility χ_{EPR}. Electron spin-lattice relaxation times T_{1e} were estimated using progressive microwave-power saturation technique.

NMR measurements were performed using a Tecmag APOLLO pulse solid-state NMR spectrometer, an Oxford Instruments 360/89 superconducting magnet (B_0=8.0196 T, f_0=85.85 MHz) and an Oxford Instruments CF1250 NMR cryostat. Measurements of the ^{13}C nuclear spin-lattice relaxation time T_{1n} were done by progressive saturation pulse sequence in the range 77 K≤T≤290 K.

3. Results

3.1. Structure of astralen nanoparticles

HRTEM provides direct evidence that astralen particles have the polyhedral multi-shell structure with a hollow inside (Fig. 1). The polyhedral faces comprise a stack of 20–50 planar graphene sheets. The intersheet distance is of ~0.340 nm. The average diameter of astralen particles is of ~40 nm.

Fig. 2(a) shows the XRD patterns of the graphite reference and astralen powder samples. The former includes narrow peaks of (002), (100), (101) and (004) crystal planes of bulk graphite. The position of the (002) peak corresponds to the conventional graphite mean inter-layer spacing d_{002} of 0.335 nm. In astralen powder sample the position of the (002) peak is shifted to the low angle direction corresponding to the mean inter-layer spacing d_{002} of 0.340 nm between the graphitic shells in the polyhedral particles. This value is completely consistent with that obtained by the HRTEM observations.

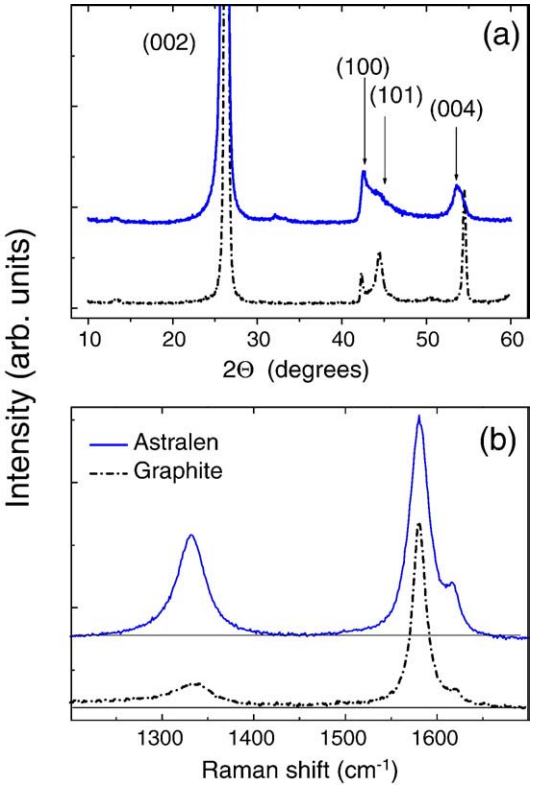

Fig. 2. XRD patterns (a) and Raman spectra (b) of the graphite reference and astralen powder samples. The profiles are shifted along the vertical axis.

Please cite this article as: A.I. Shames, et al., Diamond Relat. Mater. (2008), doi:10.1016/j.diamond.2008.10.056

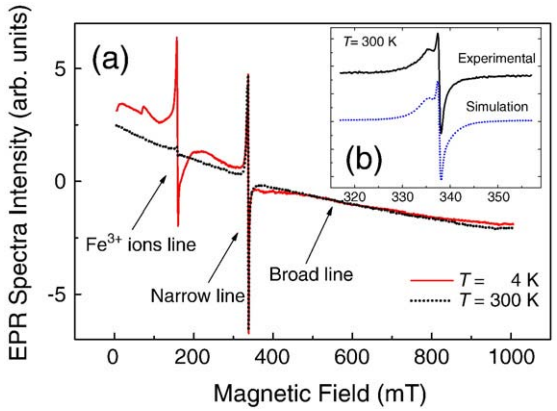

Fig. 3. EPR spectra of astralen particles: (a) general view at RT (black dotted line) and T=4 K (red solid line) recorded at the same instrumental conditions, ν=9.465 GHz; (b) asymmetric g=2.0 EPR signal at room temperature, ν=9.462 GHz, black solid line—experimental spectrum, blue dotted line—simulated spectrum, best least square fit using superposition of two Lorentzian lines. (For interpretation of the references to colour in this figure legend, the reader is referred to the web version of this article.)

Fig. 2(b) demonstrates representative Raman spectra of the graphite reference and astralen powder samples. Both spectra show two broad Raman bands around 1340 nm (D-band) and 1580 cm^{-1} (G-band). Our graphite reference and astralen powder samples demonstrated ratios between peak amplitudes I_D/I_G~0.12 and ~0.29, correspondingly.

3.2. EPR

Room temperature (RT, T=300 K) EPR spectrum of astralen particles, recorded within the maximal scan width of 1 T at incident microwave power P=20 mW and 100 kHz modulation amplitude of 1 mT, consists of two clearly distinguished components: a very broad EPR signal with the line width ΔH_{pp} exceeding 1 T and an asymmetric narrow (ΔH_{pp} of the order of several mT) signal centered close to g=2.0 (Fig. 3(a), black dotted line). The sharp low field (g~4.3) EPR line in these spectra (see Fig. 3(a)) belongs to Fe^{3+} ions originating from the capillary tube glass and is used as an external intensity reference. All spectral components (both broad and narrow ones) are found to be independent on the ambient pressure and show no changes when the sample was pumped out to the vacuum level better than 2×10^{-5} mbar at both RT and T=600 K. EPR measurements at variable temperatures were carried out on the sample sealed under vacuum. Black solid line in Fig. 3(b) shows RT spectrum of the g=2.0 EPR signal recorded within the reduced scan width of 40 mT at conditions of higher spectral resolution (modulation amplitude of 0.1 mT). This RT spectrum may be successfully simulated as superposition of two Lorentzian lines [14] of different line widths, g-factors and intensities: ΔH_{pp1}=0.67±0.01 mT, g_1=2.0034±0.0002 and ΔH_{pp2}=3.6±0.3 mT, g_2=2.007±0.001, intensities ratio DIN_2/DIN_1~13—see Fig. 3(b), blue dotted line.

EPR signals associated with astralen demonstrate unusual temperature evolution. It was found that the intensities of the broad and two g=2.0 signals, unlike EPR signals of the most paramagnetic species, do not obey the Curie law. Fig. 4 obviously demonstrate very weak changes of astralen EPR signals' intensity on decreasing temperature from T=300 K down to T=4 K whereas the EPR signal of paramagnetic Fe^{3+} ions from the sample tube, being at the same conditions as the astralen sample, shows evident temperature dependence of its intensity—see corresponding low-field signals in Fig. 3(a). Fig. 4(b) represents temperature dependences of the intensity of two overlapped astralen g=2.0 signals in comparison with that of the external reference signal from Fe^{3+} ions in capillary glass matrix. Double integration of the observable part of the very broad EPR lines with ΔH_{pp}>1 T (Fig. 3(a)), done after the subtraction of Fe^{3+} ions and narrow g=2.0 signals, evidences that these intensities are temperature independent (within the large experimental error, not shown) as well. Other parameters of the g=2.0 EPR lines demonstrate small changes on decreasing temperature.

Since possible extension of the electron spin-lattice relaxation times T_{1e} on decreasing temperature may affect the true values of the EPR lines' intensities (due to the saturation effect) the saturation curves were measured at selected temperatures. No EPR signals' saturation was observed within the temperature range under study—see Fig. 5(a). Saturation curves at all temperatures coincide with each other and are perfectly linear. Therefore T_{1e} values may be estimated as being shorter than $T_{1e}=5\times10^{-8}$ s reported for the crystalline DPPH sample [15] that reveals saturation behavior at P>50 mW—Fig. 5(a), close circles.

Amounts of paramagnetic centers observed were obtained at RT by comparison of intensities of the g=2.0 signals with the intensity of the radical-like signal in well purified nanodiamond sample with known amount of paramagnetic defects ($N_s=6.3\times10^{19}$ spins/g) [16]. Here it is worth mentioning that this astralen sample shows strong non-resonant microwave absorption, which leads to the reduction of the spectrometer's sensitivity. Thus, all data on absolute amounts of paramagnetic centers should be considered as lower limits of corresponding values and bearing an evaluative character. Amount of paramagnetic centers is found to be N_{s1}~5×10^{17} spins/g for the narrow Lorentzian line, N_{s2}~7×10^{18} spins/g for the broad Lorentzian line and, for the very broad (ΔH_{pp}>1 T) line, N_{sbr} exceeds 10^{22} spins/g (just an observable part of this line was taken for the estimation).

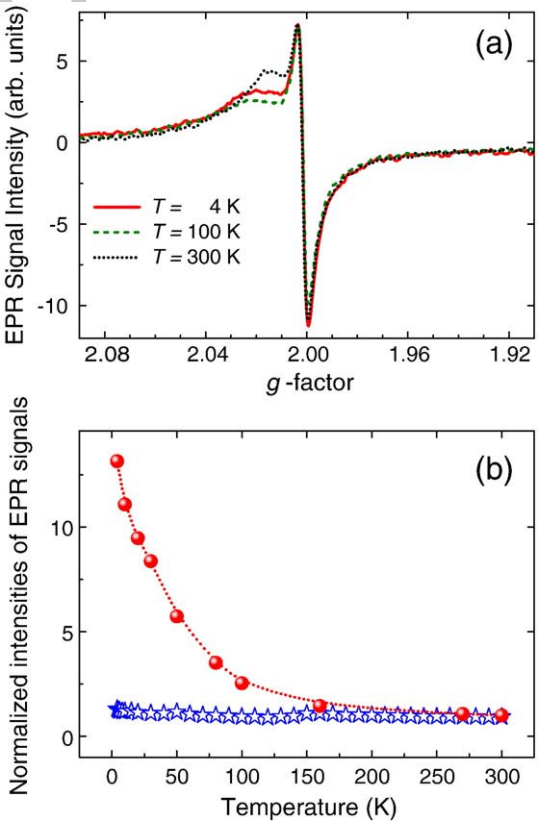

Fig. 4. (a) Narrow components of the EPR spectrum of astralen at RT (black dotted line), T=100 K (green dashed line) and T=4 K (red solid line). Spectra recorded at the same instrumental conditions; (b) DIN(T) dependences of the astralen g=2.0 EPR signals (blue stars) in comparison with the Fe^{3+} ions signal (red circles). Signal intensities are normalized to the same values at T=300 K. (For interpretation of the references to colour in this figure legend, the reader is referred to the web version of this article.)

Please cite this article as: A.I. Shames, et al., Diamond Relat. Mater. (2008), doi:10.1016/j.diamond.2008.10.056

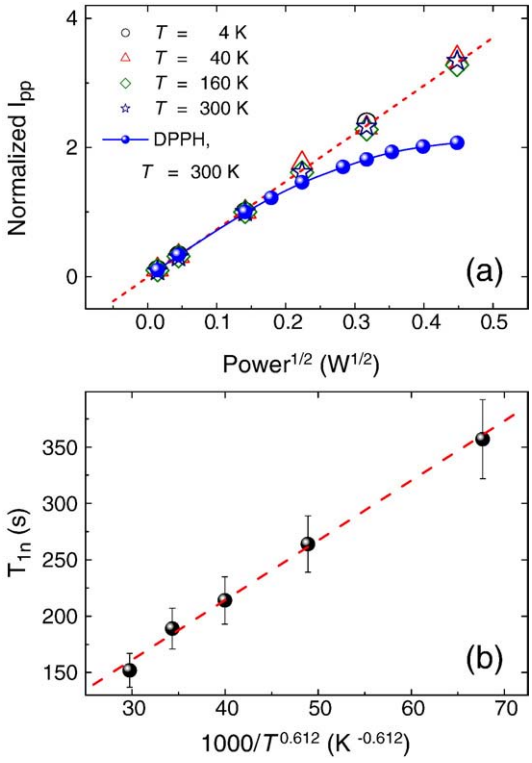

Fig. 5. (a) Microwave saturation dependences for the narrow signal at selected temperatures: circles—T=4 K, triangles up—T=40 K, diamonds—T=160 K, stars—T=300 K, dashed line—best least square linear fit. Closed circles—saturation curve for the DPPH sample, T=300 K; (b) temperature dependence of ^{13}C nuclear spin-lattice relaxation time T_{1n} in astralen.

EPR spectra of pure graphite powder (not shown) demonstrate the same general features as found in astralen samples, i.e. superposition of the very broad (ΔH_{pp}>1 T) line and the narrow asymmetric line in the region of g=2.0 (like those in Fig. 3). The asymmetric line demonstrates line shape typical for the axially symmetric g-tensor with $g_{||}$=2.031±0.005 and $g_{\perp}$=2.007±0.001 (at T=300 K). The intensity of this line also does not obey the Curie law but notably increases on decreasing temperature down to 40 K. Below 40 K the intensity starts declining.

3.3. NMR

RT ^{13}C NMR spectra of the astralen powder and the graphite reference sample evidence that the astralen spectrum is characteristic of sp^2-graphite-like carbons. Spectra of both samples show asymmetric lines due to chemical shielding anisotropy (not shown). However, the spectrum of astralen is found to be a little broader in comparison with that of graphite and its center of gravity is shifted by 15 ppm to the lower frequency. This is obviously due to a number of non-equivalent sites of carbon structure in the astralen multi-shells, e.g., non-equivalent carbon atoms, belonging to different layers in the carbon onion structure. The magnetization recovery is well fit by a stretched exponential $M(t)=M_z\{1-\exp[-(t/T_{1n})^{\alpha}]\}$, where M_z is an equilibrium magnetization. In graphite, α was found to be ~0.89, while in astralen the averaged value of α in the temperature range 77–290 K is 0.65. The ^{13}C nuclear spin-lattice relaxation time T_{1n} in graphite is found to be 106±8 s, which is close to that reported in the literature, T_{1n}=89±10 s in pristine graphite powder [17] and around 100 s in high oriented pyrolytic graphite (HOPG) [18]. RT T_{1n} value in astralen is 152±15 s. The temperature dependence of T_{1n} in the astralen sample is shown in Fig. 5(b).

4. Discussion

Our HRTEM, XRD and Raman spectroscopy studies revealed a polyhedral multi-shell fullerene-like structure of astralen particles that consist of large flat sp^2 graphene faces connected by defective corner regions with presumably pentagon-like structure. The spacing of lattice fringes of 0.340 nm is larger than the (002) inter-plane distance in graphite (~0.335 nm) but smaller than the corresponding value in polyhedral carbon onions from HTT nanodiamonds (0.345 nm [9] and 0.353 nm [7]). The large intersheet distance suggests a considerably large reduction in interlayer interaction compared to the case of bulk regular graphite. Fitting of the (002) peak of the XRD pattern of astralens (Fig. 2(a)) with the Lorentzian function gives an FWHM value of about 0.6°. It corresponds to the size of a coherent scattering region (CSR) of ~16 nm for the direction normal to the graphitic layers, calculated with the Scherrer formula. This value (47 graphene sheets) is also in accord with the HRTEM observations. The broad and asymmetric (10) peak at ~45° is caused by the superposition of the (100) and (101) peaks that can be attributed to XRD from a 2D lattice. These findings point out to the turbostratic structure and lack of 3D ordering in multi-shell astralen particles whose parallel graphitic sheets are randomly translated and rotated along the azimuth [19]. Fitting this peak by the superposition of two Lorentzian peaks (100) and (101) gives the FWHM values of 0.7° and 2.9°, for the (100) and (101) peaks, correspondingly. Thus, the CSR value calculated with the Scherrer formula in the lateral (100) direction (along the graphene plane) is L_a~15 nm.

The turbostratic structure of astralen particles is confirmed by the clearly observed change in the relative intensities of the (100), (101) and (004) peaks in astralen as compared with those for bulk graphite (Fig. 2(a)). Using the theory of X-ray scattering of carbon with turbostratic stacking structures, Fujimoto recently demonstrated [20] that relative intensities of (100) and (101) reflections are changed depending on the number of stacking graphene layers: the decrease in the number of layers leads to considerable broadening and consequent reduction of maximum intensity for (101) reflection (relative to (100) peak). The reflection (004 is) also broadened and shifted towards small diffraction angles. Since the number of stacking layers in astralene sample is essentially less than in the bulk graphite the relative intensities of above peaks are changed in comparison with regular graphite—see Fig. 2(a).

Raman spectra of astralen samples (Fig. 3) include broad bands around 1340 and 1580 cm^{-1}. The band at about 1580 cm^{-1} (G-band) corresponds to the E_{2g} mode in the graphite structure. Ideal single-crystalline graphite should show only the G-band in the spectrum range from 1200 to 1700 cm^{-1} [21]. In addition to the G-band, so-called D-band appears at about 1340 cm^{-1} for finite-size or disordered graphite-like samples (e.g. polycrystalline graphite, glassy carbon, etc.). The true origin of the D-band in graphite-like materials is still under discussion [22,23]. However, it was empirically shown that a modest amount of disorder and the resultant decrease in an in-plane domain size (L_a) of the graphitic sp^2 sheets could give rise to the D-band [19,24]. Accordingly, the relative intensity of the D- to G-bands (I_D/I_G) is widely used for a qualitative representation of L_a in graphite-like samples in general and carbon onions, in particular [5,7]. Using the empirical formula $L_a \approx 4.4\times(I_G/I_D)$ we estimate the L_a in-plane size of ~15 nm. This value is consistent with the corresponding L_a size obtained by XRD and the average size of the flat faces of polyhedral astralen particles revealed by HRTEM. Therefore, we suggest that these carbon nanoparticles have defect-free sp^2 flat faces and all of the defects condense at their polyhedral edges.

In-plane dimensions of defect-free sp^2 flat faces in astralen particles are considerably larger than that for the best polyhedral carbon onions originated from HTT nanodiamonds: 3.6 nm [9] and 7 nm [7]. On the other hand, it should be noted that giant polyhedral

Please cite this article as: A.I. Shames, et al., Diamond Relat. Mater. (2008), doi:10.1016/j.diamond.2008.10.056

carbon particles with size of flat faces up to 100 nm were recently synthesized by laser ablation [25] and DC arc vaporization [26] of graphite. Unfortunately, electronic properties of these particles have note been reported.

Let us consider the magnetic resonance data obtained for astralens, again—in the view of the results and conclusions drawn from the thorough studies of quasi-spherical and polyhedral carbon onions originated from HTT nanodiamonds [5,7–9].

Except of the very the broad EPR line with $\Delta H_{pp}>1$ T, both relatively narrow signals with $g=2.0$ revealed in our study have also been observed in EPR spectra of various HTT nanodiamonds. Thus, narrow ($\Delta H_{pp}\sim 0.7$–0.9 mT) Lorentzian lines with $g=2.0020$–2.0022 which intensities obey the Curie law have been found in quasi-spherical carbon onions obtained by "soft" thermal treatment [5,9]. Broad ($\Delta H_{pp}\sim 1$–10.9 mT, depending on the oxygen pressure) Lorentzian lines with $g=2.0010$–2.0014, which intensities show features characteristic of Pauli or mixed Pauli–Curie paramagnetism, have been found in small polyhedral particles obtained by more intensive thermal treatment [7,9]. These relatively broad EPR signals were attributed to non-bonding π-electrons localized at the marginal regions of a nanographite sheet having a zigzag shape [9].

In general, the $g=2.0$ EPR signals found in astralen (Fig. 3) look like signals of the aforementioned types. The Lorentzian shape of the narrow EPR lines is quite natural for de-aggregated conducting carbon nanoparticles where particle dimensions are smaller than skin depth at ~9.4 GHz. However, there are several noteworthy differences found for the signals in astralen in comparison with those observed in carbon onions produced by HT treatment of nanodiamonds:

(i) Both EPR signals in astralen do not depend on oxygen pressure whereas the broad EPR signals in polyhedral nanographite were found to be very sensitive to the oxygen pressure. Indeed, we found that reduction of oxygen pressure does not affect the line widths for all EPR signals observed in astralen. Broadening of the EPR signals due to the spins localized at the edge states in an oxygen atmosphere has been studied in detail and is considered to be due to dipole–dipole and exchange interactions between the paramagnetic dioxygen molecules and the spins localized at edges and/or other defects [9,27,28]. It means that at ambient conditions oxygen molecules cannot penetrate through the graphene sheets of astralen particles. This finding is an accord with an absence of HRTEM observations of any structural voids or discontinuities in the graphene layers of astralens;

(ii) intensities of all EPR signals do not depend on temperature within the very broad temperature range, i.e. demonstrate the Pauli paramagnetism (Fig. 4). Only the narrow $g=2.0$ signal demonstrates a very weak Curie-like behavior at approaching $T=4$ K;

(iii) g-factor values measured for the broad and narrow Lorentzian lines in astralen are found to be higher than those for HTT nanodiamonds: 2.0034 vs. 2.0022 and 2.007 vs. 2.0013 for the narrow and broad signals at RT, respectively.

Following [9], we suppose that the electronic properties of nanographite systems including its magnetic and conducting characteristics depend on sizes of defect-free domains in graphene sheets, L_α. Furthermore, in astralen the size of these defect-free domains coincides with the size of flat grapheme faces. On the other hand, the L_α is comparable (and even exceeds) the known size for nano-graphite particles exhibiting an abrupt transition (in the range of 5–15 nm) to the bulk graphite properties [29].

The most unusual feature of EPR properties observed in astralen is the Pauli-type behavior of EPR magnetic susceptibilities for all signals in the wide temperature range, especially in the low-temperature region 4–50 K (Fig. 4). Such a behavior has never been observed in EPR studies done on multi-shell nanocarbon samples. Thus, nanodiamond-derived onion-like and polyhedral nanoparticles demonstrated the Curie–Weiss behavior below 100 K for both narrow and broad lines with the Curie-type contribution originating from localized sp^3 spins (narrow lines) and the enhanced Pauli-type contribution originating from non-binding π-electron states spins localized at the zigzag edges (broad lines) [7,8]. It was shown that the spin paramagnetism associated with the edge state behaves as a temperature-dependent Curie-type or an enhanced Pauli-type temperature independent susceptibility according to the feature of the edge state [9]. The interaction of the edge state with the conduction band carriers creates the Pauli-type behavior and the structural disorder leads to the Curie-type localized nature for the edge-state spins. However, unlike the case of quasi-spherical or small polyhedral onions produced by HTT of nanodiamonds, where the treatment conditions determine the observed features of paramagnetic behavior for the edge-state spins, in astralen not only itinerant spins (the very broad line) but also quasi-localized spins (the narrow line) show the same Pauli-type behavior down to 4 K. We may suppose that in astralen both the quasi-localized and the localized spins are associated with the corner-condensed defects and interact with numerous conduction electrons which belong to the same graphene layer of the astralen particle. Just this interaction, in our opinion, is responsible for unusual properties of EPR active spins observed in astralen samples and can be understood within the framework of the well-developed theory of electron resonance of localized electron spins in metals [30,31]. Following this theory the main factor determining all electron magnetic resonance features is the ratio of magnetic susceptibilities of conduction electrons χ_s and localized paramagnetic centers χ_d: $\chi_r=\chi_d/\chi_s$. In the cases of $\chi_r \ll 1$ the conduction electrons properties will predominate and EPR signals of localized paramagnetic centers will behave in the same manner as signals of conduction electrons spin resonance (CESR), i.e. their intensities will demonstrate the Pauli-type paramagnetism. When $\chi_r>1$ properties of EPR signal will be determined by properties of localized paramagnetic centers, that is the Curie-type paramagnetism. Thus, the aforementioned assumption on the high value of ratio between the numbers of delocalized π-electrons and localized and quasi-localized spins in astralen system exhaustively explains the unusual temperature dependences of the EPR signals observed in astralen. Several experimental observations support this assumption. First of all, the aforementioned strong non-resonant microwave absorption found (which leads to the Q-value reduction) is a characteristic feature for all conduction graphite samples. Another argument in favor of the presence of a large amount of conduction electrons may be the very broad ($\Delta H_{pp}>1$ T) EPR signals that have been observed in both astralen and conducting graphite samples. It is well known that in the most of metals CESR lines may be so broad that CESR is not observable [30,31]. Observation of broad EPR signals in natural graphite powder was reported in ref. [32]. Quite broad (>0.1 T) CESR signals were observed in Rb_3C_{60} system [33] and doped chalcogenide nanotubes [34]. Thus, very broad CESR lines are not uncommon ones for carbon-based and nano-sized systems. An alternative explanation of this EPR line may be low (below the XRD detection threshold) abundance of ferromagnetic impurities. However, typical ferromagnetic impurities in nano-carbon samples reveal much narrower EPR line [28,35]. Moreover, it is hard supposing the same impurities (responsible for the same very broad EPR lines) appear in both astralen and commercial pure graphite. Taking into account all aforementioned speculations the attribution of the very broad EPR line to CESR sounds quite reasonable.

Let us estimate the number of different spins per each astralen particle. The bottle density of astralen was found to be 2.2 ± 0.1 g/cm^3 [10]. The average diameter of an astralen particle is 40 nm which gives the weight of a single astralen particle 7.38×10^{-17} g. Thus each astralen particle contains (totally, in all graphene layers) ca. 40 of localized spins, ca. 500 of quasi-localized spins and above 10^6 of spins

Please cite this article as: A.I. Shames, et al., Diamond Relat. Mater. (2008), doi:10.1016/j.diamond.2008.10.056

responsible for the CESR signal. The presence of such an amount of conduction (delocalized) π–electrons per each astralen nanoparticle perfectly complies with the condition $\chi_r \ll 1$ and dictates the distinctly pronounced Pauli-type behavior for intensities of all EPR signals observed.

The temperature-dependent ^{13}C NMR relaxation data in astralen supplies additional arguments in favor of the aforementioned hypothesis. Relaxation measurements on pristine graphite powder done at 1.3–4.2 K and room temperature, made by Carver [17], led to $T_{1n} \sim T^{-0.7}$ dependence. The same measurements on astralen in the range of 77 to 290 K yield $T_{1n} \sim T^{-0.612}$ (Fig. 5(b)). The fitting result shows that the slope value in the temperature dependence of T_1 falls between the metallic behavior, $T_{1n} \sim T^{-1}$ (Korringa relation), and the semiconductor behavior, $T_{1n} \sim T^{-0.5}$.

Finally, both EPR and NMR experiments justify the following model of the electron system in astralen. Each large multi-shell carbon polyhedron contains: (a) relatively small (ca. 40) number of localized spins; (b) quasi-localized π-electron state spins (ca. 500); (c) spins of delocalized (conduction) π–electrons (above 10^6). Both localized and quasi-localized spins are condensed near the corners of the astralen polyhedra.

5. Conclusions

We report unusual electronic and magnetic features of the astralen nanoparticles and discuss them in terms of the hypothesis that each stralen nanoparticle constitutes a closed network of delocalized π-electrons. This feature is attributed to the multi-shell polyhedral structure of astralen and in particular to the fact that the polyhedra consist of large (~15 nm) defect-free sp^2 flat faces while limited number of the defects condense at the polyhedral edges.

Acknowledgements

This work was supported, in part, by the Israeli Ministry of Immigrant Absorption and the New Energy Development Organization of Japan (NEDO, grant # 04IT4). The authors acknowledge Dr. L. Zeiri for her help with Raman measurements.

References

[1] H.W. Kroto, J.R. Heath, S.C. O'Brien, R.F. Curl, R.E. Smalley, Nature 318 (1985) 162.
[2] L. Euler, Novi corumentarii academie Petropolitanae, 4 (1752/3) 109.
[3] D. Ugarte, Nature 359 (1992) 707.
[4] H. Terrones, M. Terrones, J. Phys. Chem. Solids 58 (1997) 1789.
[5] S. Tomita, T. Sakurai, H. Ohta, M. Fujii, S. Hayashi, J. Chem. Phys. 114 (2001) 7477.
[6] P.V. Pikhitsa, Y.J. Kim, M.W. Kim, S. Yang, T.W. Noh, M. Choi, Phys. Rev. B 71 (2005) 073402.
[7] O.E. Andersson, B.L.V. Prasad, H. Sato, T. Enoki, Y. Hishiyama, Y. Kaburagi, M. Yoshikawa, S. Bandow, Phys. Rev. B 58 (16) (1998) 387.
[8] B.L.V. Prasad, H. Sato, T. Enoki, Y. Hishiyama, Y. Kaburagi, M. Yoshikawa, A.M. Rao, P. C. Eklund, M. Endo, Phys. Rev. B 62 (2000) 11209.
[9] V.Yu. Osipov, T. Enoki, K. Takai, K. Takahara, M. Endo, T. Hayashi, Y. Hishiyama, Y. Kaburagi, A. Ya Vul', Carbon 44 (2006) 1225.
[10] Layered fulleroid-type polyhedral carbon nanostructures. Ponomarev A.N., Nikitin V.A., Patent RU 2196731 from 2000.09.21 filed on 2003.01.20.
[11] O.B. Danilov, I.M. Belousova, A.A. Mak, V.P. Belousov, A.S. Grenishin, V.M. Kiselev, A. V. Kris'ko, T.D. Murav, eva, A.N. Ponomarev, E.N. Sosnov, SPIE Proc 5777 (2005) 270.
[12] I.M. Belousova, V.P. Belousov, O.B. Danilov, A.V. Ermakov, V.M. Kiselev, A.V. Kris, ko, T.D. Murav, eva, A.N. Ponomarev, E.N. Sosnov, SPIE Proc 5777 (2005) 277.
[13] M.A. Belyaeva, M.V. Gryaznova, V.V. Danilov, A.N. Ponomarev, V.V. Ryl, kov, SPIE Proc. 5990 (2005) 59900H–1.
[14] C.P. Poole, Electron Spin Resonance: A Comprehensive Treatise on Experimental Techniques, Second ed.Courier Dover Publications, 1996 Chapter 12.
[15] G.P. Goldsborough, M. Mandel, G.E. Pake, Phys. Rev. Lett. 4 (1960) 13.
[16] V.Yu. Osipov, A.I. Shames, T. Enoki, K. Takai, M.V. Baidakova, A. Ya Vul, Diamond Relat. Mater. 16 (2007) 2035–2038.
[17] G.P. Carver, Phys. Rev. B 2 (1970) 2284.
[18] K. Kume, Ann. de Phys. 11 (1986) 245.
[19] J. Robertson, Adv. Phys. 4 (1986) 317.
[20] H. Fujimoto, Carbon 41 (2003) 1585.
[21] F. Tuinstra, J.L. Koenig, J. Chem. Phys. 53 (1970) 1126.
[22] H. Wilhelm, M. Leaurain, E. McRae, B. Humbert, J. Appl. Phys. 84 (1998) 6552.
[23] M.J. Matthews, M.A. Pimenta, G. Dresselhaus, M.S. Dresselhaus, M. Endo, Phys. Rev. B 59 (1999) R6585.
[24] D.S. Knight, W.B. White, J. Mater. Res. 4 (1989) 385.
[25] F. Kokai, A. Ishihara, A. Koshio, A. Nakayama, Y. Koga, Diamond Relat. Mater. 16 (2007) 1264.
[26] X. Song, Y. Liu, J. Zhu, Mater. Lett. 61 (2007) 4781.
[27] S. Bandow, F. Kokai, K. Takahashi, M. Yudasaka, S. Iijima, Appl. Phys. A 73 (2001) 281.
[28] A.I. Shames, A.M. Panich, E. Mogilko, J. Grinblat, E.W. Prilutskiy, E.A. Katz, Diamond Relat. Mater. 16 (2007) 2039.
[29] H.T. Pinnick, Phys. Rev. 94 (1954) 319.
[30] J.H. Pifer, R.T. Longo, Phys. Rev. B 4 (1971) 3797.
[31] J. Winter, Magnetic Resonance in Metals, Clarendon Press, Oxford, 1971 Chapter 10.
[32] K. Matsubara, T. Katsuramaki, K. Kawamura, T. Ema, Tanso 175 (1996) 249.
[33] A. Jánossy, O. Shauvet, S. Pekker, J.R. Cooper, L. Forró, Phys. Rev. Lett. 71 (1993) 1091.
[34] D. Arčon, A. Zorko, P. Cevc, A. Mrzel, M. Remškar, R. Dominko, M. Gaberšček, D. Mihailović, Phys. Rev. B 67 (2003) 125423-1.
[35] A.I. Shames, A.M. Panich, W. Kempiński, A.E. Alexenskii, M.V. Baidakova, A.T. Dideikin, V.Yu. Osipov, V.I. Siklitski, E. Osawa, M. Ozawa, A. Ya Vul, J. Phys. Chem. Solids 63 (2002) 1993.

Please cite this article as: A.I. Shames, et al., Diamond Relat. Mater. (2008), doi:10.1016/j.diamond.2008.10.056